Available online at www.sciencedirect.com

SciVerse ScienceDirect

Ceramics International 39 (2013) 1403–1411

CERAMICS INTERNATIONAL

www.elsevier.com/locate/ceramint

Physical properties and electrochemical performance of molybdenum–lead-germanate glasses and glass ceramics

S. Rada[a], E. Culea[a,*], R. Chelcea[a], M. Rada[b], A. Bot[b], N. Aldea[b], V. Rednic[b]

[a]Department of Physics & Chemistry, Technical University of Cluj-Napoca, 400020 Cluj-Napoca, Romania
[b]National Institute for R&D of Isotopic and Molecular Technologies, Cluj-Napoca 400293, Romania

Received 6 July 2012; received in revised form 24 July 2012; accepted 24 July 2012
Available online 3 August 2012

Abstract

Glasses and glass ceramics of the $xMoO_3(100-x)[7GeO_2 \cdot 3PbO]$ system where $x=0$–30 mol% MoO_3 were synthesized and characterized in order to obtain information about the structural correlations and the relationship between structure and physical properties in these materials. Changes of the FTIR, UV–vis and EPR data are discussed in view of the glass network structural changes determined by the evolution of molybdenum ions state, glass composition and MoO_3 concentration.

The spectroscopic studies indicate that with increasing of MoO_3 content a fraction of the Mo^{6+} ions convert Mo^{3+} and Mo^{5+} ions. Accordingly, these modifications cause the depolymerization of the host network, the increase of the structural disorder and formation of GeO_2 and $PbMoO_4$ crystalline phases. The shape of EPR spectra is modified by the increase of the MoO_3 concentration indicating that molybdenum ions exists in glass and glass ceramics in more than one valence state. The EPR spectra contain a broad line located at $g \sim 5.2$ and, for the samples with a MoO_3 content up to $x \geq 15$ mol%, the presence of the hyperfine structure characteristic for the Mo^{5+} ions can be observed, too.

The electrochemical performances of the glass and glass ceramics samples with $x=10$ and 30 mol% MoO_3 were demonstrated by cyclic voltammetry.

Keywords: B. Spectroscopy; D. Glasses; Voltammetry; DFT calculations

1. Introduction

MoO_3 is a transition metal oxide, belonging to the intermediate class of glass forming oxides which may participate in the glass network forming in the presence of modifier oxides like PbO, but it may also act as a modifier [1]. In the case of molybdenum–phosphate glasses the different oxidation states for molybdenum ions were found to coexist [2]. Moreover, glasses containing molybdenum ions have interesting optical and electrical properties depending on the type and composition of glass and the different valence states of molybdenum ions [3]. Such peculiar properties are related to the ability of molybdenum ions to exist in glasses in four possible valences, namely Mo^{3+}, Mo^{4+}, Mo^{5+} and Mo^{6+} [4–6]. The conductivity process in transition metal ion glasses, such as Mo, V, etc. can be interpreted by the small polaron model in which the electronic conduction can occur through the electronic transfer from the low- to high-valence states which is in agreement with Refs. [7–10]. The electrical conduction can take place by a transfer of electrons from Mo^{5+} to Mo^{6+} ions [4]. The Mo^{6+} ions participate in the glass network within the $[MoO_4]$ and $[MoO_6]$ structural units while the Mo^{5+} ions act as modifiers. These mixed ionic–electronic conductor glasses have become a current topic mainly in applications such as electrochemical cells, high-density memories, smart windows, electro-optical and electrochromic devices [11,12]. On the other hand, it is known that the Mo^{5+} ions are a sensitive indicator for the structural changes of the local symmetry in oxide glasses [13].

It is well known that lead oxide is unique in its influence on the glass structure [14,15] and is widely used in glasses because it enhances the resistance against devitrification, improves the chemical durability and lowers the melting

*Corresponding author.
E-mail address: eugen.culea@phys.utcluj.ro (E. Culea).

0272-8842/$ - see front matter © 2012 Elsevier Ltd and Techna Group S.r.l. All rights reserved.
http://dx.doi.org/10.1016/j.ceramint.2012.07.082

temperature [13]. Despite several detailed investigations, the structure of lead germanate glasses appears to be, as yet, not fully understood. In particular, different authors have different points of view about the presence of six-fold coordinated germanium atoms in lead-germanate glasses [16]. Moreover, the local structure of Pb^{2+} ions has not been definitely established.

In order to obtain further information on the local symmetry and interaction between metallic ions in oxide glasses, we studied some lead-germanate glasses containing molybdenum ions. Thus, glass and glass ceramics with the $x MoO_3 \cdot (100-x)[7GeO_2 \cdot 3PbO]$ composition, where $x=0$–30, were prepared by a classical melt quenching technique and were characterized by density measurements, DFT calculations, cyclic voltammetry, FTIR, UV–vis and EPR spectroscopy. Moreover, this study is extended in order to study the effect of MoO_3 concentration on structural, optical, electrochemical properties and to justify the induced modifications and the status of molybdenum ions in the host lead germanate glass and glass ceramics.

2. Experimental

Glasses were prepared using reagent grade purity germanium (IV) oxide, lead (II) oxide and molybdenum (VI) oxide of high purity in suitable proportions. The mechanically homogenized mixtures were melted in sintered corundum crucibles at 1000° C in an electric furnace. The samples were put into the electric furnace directly at this temperature. After 10 min, the molten material was quenched at room temperature by pouring onto a stainless-steel plate.

The samples were analyzed by means of X-ray diffraction using a XRD-6000 Shimadzu diffractometer, with a monochromator of graphite for the Cu-Kα radiation ($\lambda=1.54$ Å) at room temperature.

The FTIR spectra of the glasses in the 350–1200 cm^{-1} spectral range were obtained with a JASCO FTIR 6200 spectrometer using the standard KBr pellet disc technique. The spectra were carried out with a standard resolution of 2 cm^{-1}.

UV–visible absorption spectra of the powdered glass samples were recorded at room temperature in the 250–11,000 nm range using a Perkin-Elmer Lambda 45 UV/VIS spectrometer equipped with an integrating sphere. These measurements were made on glass powder dispersed in KBr pellets. The validity of the band position is ± 2 nm.

EPR measurements were performed at room temperature using an ADANI portable EPR PS 8400-type spectrometer, in the X frequency band (9.1 GHz) and a field modulation of 100 kHz. The microwave power was 5 mW.

The starting structures have been built using the graphical interface of Spartan'04 [17] and preoptimized by molecular mechanics. Optimizations were continued at DFT level (B3LYP/CEP-4G/ECP) using the Gaussian'03 package of programs [18].

It should be noticed that only the broken bonds at the model boundary were terminated by hydrogen atoms. The positions of boundary atoms were frozen during the calculation and the coordinates of internal atoms were optimized, to model the active fragment flexibility and its incorporation into the bulk.

The electrochemical properties were characterized by cyclic voltammetry using a VERSASTAT3 potentiostat and V3Studio software. Discs of glasses were used as working electrode, platinum electrode as counter and calomel as reference electrode.

3. Results and discussion

The diffraction patterns of glasses and glass ceramics with $x=20$–30 mol% MoO_3 are presented in Fig. 1. The X-ray diffraction patterns did not reveal any crystalline phase in the samples with $x<20$ mol% MoO_3. Then, in the sample with $x=25$ mol% MoO_3, the presence of the GeO_2 crystalline phase (tetragonal system) was detected. By increasing the MoO_3 content up to 30 mol%, X-ray diffraction patterns show the apparition of GeO_2 and $PbMoO_4$ crystalline phases.

3.1. Density, molar volume and oxygen packing density

A simple inspection of the density, molar volume (V_m) and oxygen packing density (d_O) data suggests that the gradual addition of molybdenum ions generates changes of the basic structural units of the glass matrix. From Fig. 2, it is observed that increasing the molybdenum content of the samples determines an almost linear decrease of the molar volume. This decrease is associated with a decrease in the number of non-bridging oxygens and with a contracting effect of the network due to the formation of

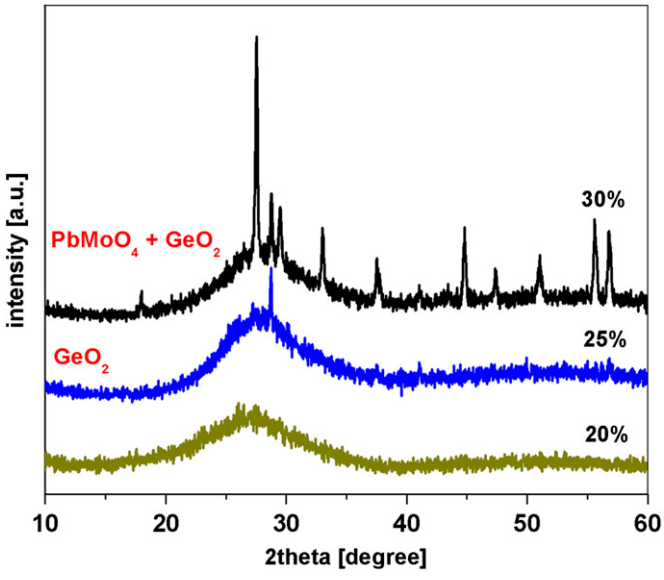

Fig. 1. X-ray diffraction patterns for $xMoO_3(100-x)[7TeO_2 \cdot 3PbO]$ samples where $x=20$, 25 and 30 mol%.

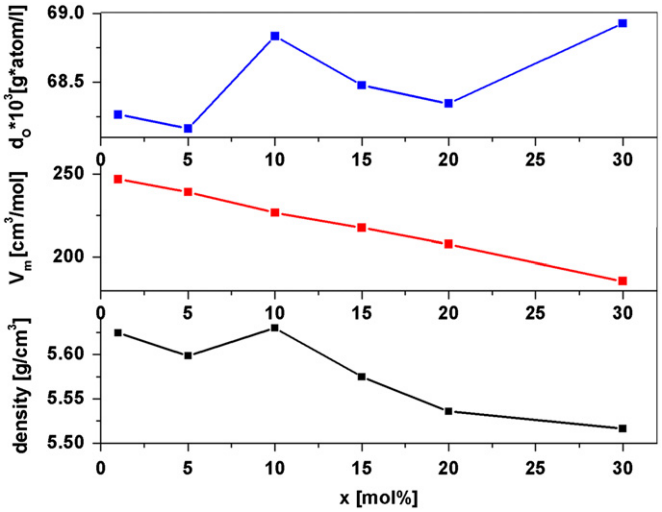

Fig. 2. Compositional dependence of density, d (a), molar volume, V_m (b) and the oxygen packing density, d_O (c) for xMoO$_3$(100 − x)[7TeO$_2$ · 3PbO] samples where x=20, 25 and 30 mol%.

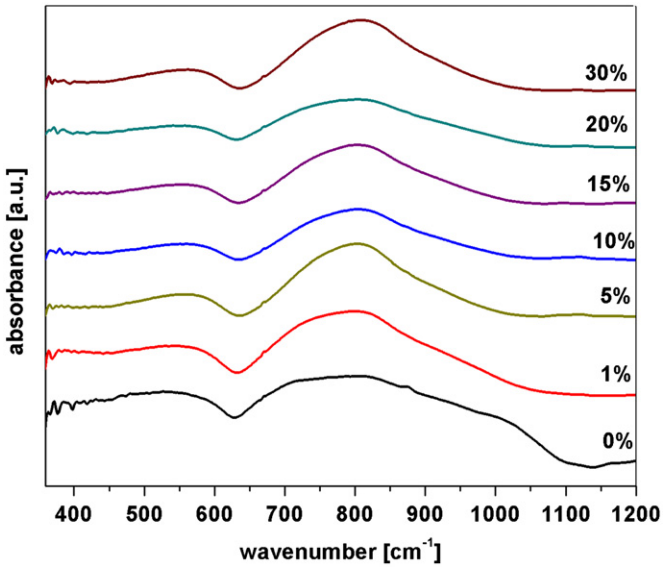

Fig. 3. FTIR spectra of the xMoO$_3$(100 − x)[7TeO$_2$ · 3PbO] system where $0 \le x \le 30$ mol% MoO$_3$.

[GeO$_6$] structural units which are slightly larger in size than the [GeO$_4$] species.

The composition dependence of the density is shown in Fig. 2(a). The density decreases from 5.63 (for x=10 mol% attaining maximum value) to 5.51 g/cm^3 (for x=30 mol% MoO$_3$). For the sample with x=10 mol% MoO$_3$, the formation of [GeO$_6$] octahedral structural units in the network results in better packing and hence the increase of density.

By increasing the MoO$_3$ content up to 15 mol%, the molybdenum ions entered the glass network in the interstitial vacancies. These act to decrease gradually the oxygen free volume in the molybdenum–lead-germanate glass network and thus, also the density was observed to decrease. Accordingly, the progressive increase of the MoO$_3$ content caused a decrease in the density; this is indicative of decreasing structural compactness of the material. In general, the structural compactness, the modification of the geometrical configuration of the glassy network, the change in the coordination of the glass forming ions and the fluctuations in the dimensions of the interstitial holes are the factors that influence the density of the glass ceramic material.

3.2. FTIR spectroscopy

Fig. 3 illustrates the compositional evolution of the FTIR spectra of molybdenum–lead-germanate glasses and glass ceramics containing varying MoO$_3$ contents. These changes can be summarized as follows:

(i) The stronger IR absorption band centered at about ~800 cm^{-1} was assigned to the Ge–O stretching vibrations of [GeO$_4$] structural units [19–21] and the Mo–O stretching vibrations of [MoO$_4$] structural units [22–24].

(ii) By increasing the MoO$_3$ content up to 20 mol%, the intensity of the IR band centered at about 920 cm^{-1} and due to the Mo–O stretching vibrations of [MoO$_6$] structural units becomes more formed.

(iii) By increasing the MoO$_3$ content up to 10 mol%, the IR band situated at about 700 cm^{-1} and assigned to the stretching vibrations of the Ge–O bonds of [GeO$_6$] structural units become somewhat more pronounced. The number of [GeO$_6$] structural units cannot grow by increasing of MoO$_3$ content because the excess oxygen will coordinate with [MoO$_n$] structural units (where n=4, 6).

The structure of the base glass is characterized by a large number of non-bridging oxygens and therefore is relatively open. The observations presented above show that by increasing the MoO$_3$ content of samples up to 10 mol%, the [GeO$_4$] tetrahedral structural units were converted into [GeO$_6$] octahedral structural units up to a maximum. In this manner the excess oxygen added to the glass by the addition of MoO$_3$ is taken up by forming isolated [GeO$_6$] octahedral structural units. The further increase of the MoO$_3$ content is followed by a reconversion of Ge(VI) into Ge(IV) and Ge(V) with the simultaneous formation of non-bridging oxygens. This hypothesis is in agreement with XRD data which show that by increasing of MoO$_3$ content up to 25 mol%, the GeO$_2$ crystalline phase in tetragonal system was detected. The excess of oxygen can be accommodated in the host network by the formation of the [MoO$_n$] structural units (where n=4 and 6). In brief, lead ions ionically bonded will have a strong affinity towards [GeO$_5$] structural units containing non-bridging oxygens and [MoO$_4$]$^{2-}$ molybdate units. The pronounced affinity towards molybdate anions yields the formation of the PbMoO$_4$ crystalline phase. At first stage, the

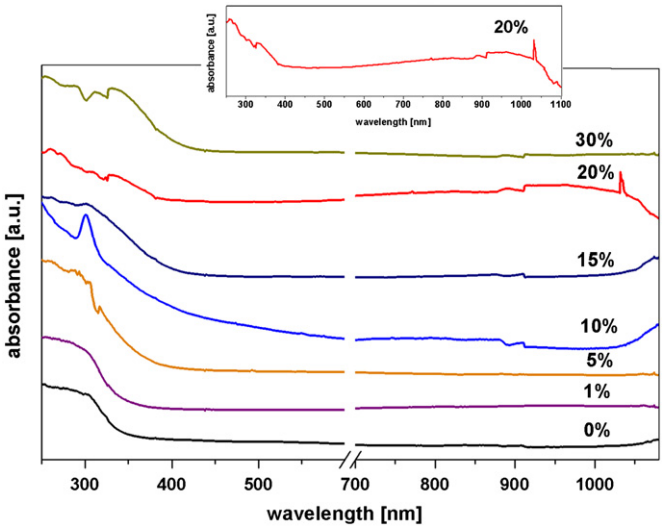

Fig. 4. UV–vis absorption spectra of the $x\mathrm{MoO_3}(100-x)[7\mathrm{TeO_2}\cdot 3\mathrm{PbO}]$ system where $0 \le x \le 30$ mol% $\mathrm{MoO_3}$.

molybdenum ions enter the glass network in positions related to $[\mathrm{MoO_4}]$ structural units and also as network modifiers in $[\mathrm{MoO_6}]$ structural units.

3.3. UV–vis spectroscopy

Molybdenum ions are expected to exist both in $\mathrm{Mo^{6+}}$ and $\mathrm{Mo^{5+}}$ valence states in the glass network due to the observed color modifications of the samples. When the concentration of $\mathrm{MoO_3}$ in the glass network is increased, the color of the glasses was observed to change from pale yellow to thick yellow, indicating the reduction of a fraction of molybdenum ions from the $\mathrm{Mo^{6+}}$ (colorless, diamagnetic ion) to the $\mathrm{Mo^{5+}}$ ($4d^1$ paramagnetic ion) valence state. The $\mathrm{Mo^{5+}}$ ions are quite stable and occupy octahedral position with distortion due to the Jahn–Teller effect [25]. The magnetic properties of the studied glasses obviously arise from the presence of $\mathrm{Mo^{5+}}$ ions.

Fig. 4 shows the UV–vis spectra of molybdenum–lead-germanate glasses and glass ceramics containing different concentrations of $\mathrm{MoO_3}$. With increasing concentration of molybdenum ions there is a gradual increase in the intensity of these bands, attaining a maximum for the sample with $x=20$ mol% $\mathrm{MoO_3}$. With the addition of $\mathrm{MoO_3}$ to the host network, the absorption edge is found to be shifted gradually towards higher wavelength side.

An examination of the spectra from Fig. 4 shows that the characteristic UV–vis bands are modified by the addition of $\mathrm{MoO_3}$ as follows:

(i) For glasses with $x \le 5$ mol% $\mathrm{MoO_3}$, the UV absorption bands are assumed to originate from the lead-germanate host matrix and the charge transfer transitions due to the $\mathrm{Mo^{6+}}$ ions. Smaller absorption band located at about 320 nm can be related to $\mathrm{Mo^{3+}}$ ions [5,6], in agreement with the EPR data. A highly possible mechanism can be summarized as follows:

$$2\mathrm{Mo^{6+}} + 3\mathrm{Pb^{2+}} \rightarrow 2\mathrm{Mo^{3+}} + 3\mathrm{Pb^{4+}}$$

These typical modifications of the glass network are supported by our FTIR data (the gradual disappearance of characteristic bands of the $[\mathrm{PbO_3}]$ structural units located at about 1050 $\mathrm{cm^{-1}}$) and EPR spectra (the resonance line attributed to the $\mathrm{Mo^{3+}}$ ions is located at about $g\sim 5.2$).

(ii) For the sample with $x=10$ mol% $\mathrm{MoO_3}$, the degree of polymerization increases. This structural evolution can be explained by the conversion of some $[\mathrm{GeO_4}]$ into $[\mathrm{GeO_6}]$ structural units, which is driven by the need to accommodate additional oxygen in the glass system. It is possible that the number of $[\mathrm{GeO_6}]$ structural units to attain maximum value, in agreement with density value and with the increase of intensity of the IR band located at about 700 $\mathrm{cm^{-1}}$. Noticeable changes appear in the intensity of the UV–vis bands centered at about 310 nm which corresponds to the $\mathrm{Pb^{2+}}$ ions with s^2 configuration and also in the intensity of the bands located in the region between 450 and 580 nm which can be related to $\mathrm{Mo^{4+}}$ ions [5,6]. On the other hand, the decrease in intensity of the EPR resonance line located at about $g\sim 5.2$ is related to the oxidation of some $\mathrm{Mo^{3+}}$ ions into $\mathrm{Mo^{4+}}$ ions. A possible mechanism which explains the scheme of the structural modifications is represented on the basis of following equation:

$$2\mathrm{Mo^{3+}} + \mathrm{Pb^{4+}} \rightarrow 2\mathrm{Mo^{4+}} + \mathrm{Pb^{2+}}$$

(iii) By increasing the $\mathrm{MoO_3}$ concentration up to 15 mol%, the presence of $\mathrm{Mo^{5+}}$ ions was detected by EPR spectroscopy investigations. The following redox reactions can be proposed:

$$\mathrm{Mo^{6+}} + 1\mathrm{e^-} \rightarrow \mathrm{Mo^{5+}}$$

$$2\mathrm{Mo^{4}} + -2\mathrm{e^-} \rightarrow 2\mathrm{Mo^{5+}}$$

$$\mathrm{Mo^{3+}} - 1\mathrm{e^-} \rightarrow \mathrm{Mo^{4+}}$$

$$\mathrm{Pb^{4+}} + 2\mathrm{e^-} \rightarrow \mathrm{Pb^{2+}}$$

These modifications are supported by the decrease in the intensity of the UV–vis band associated to electronic transitions of the $\mathrm{Mo^{4+}}$ ions and the decrease in the intensity of the EPR resonance line located at about $g\sim 5.2$. The appearance of small hyperfine structure characteristic of $\mathrm{Mo^{5+}}$ ions shows that a number of $\mathrm{Mo^{6+}}$ ions changed into $\mathrm{Mo^{5+}}$ ions due to the reducing character of glasses and some $\mathrm{Mo^{4+}}$ or $\mathrm{Mo^{3+}}$ ions oxidized to $\mathrm{Mo^{5+}}$ ions.

(iv) With the progressive increase of the $\mathrm{MoO_3}$ content up to 20 mol%, the intensity of the UV–vis absorption bands attains a maximum value. The spectra retain bands with the same absorption intensity in the UV-region and with a gradual increase in the visible domain located in the region between 400 and 1100 nm. The ultraviolet absorption bands located in

the 320–385 nm region can be correlated with the contribution of Pb^{2+} ions [11]. In the visible region, the band recorded at 850–860 nm can be assigned to Mo^{5+} ions. The Mo^{5+} ions produce two bands in the 360–380 and 710–780 nm ranges [11].

The growth of these bands reveals the presence of Mo^{5+} ions. The oxidation and reduction processes of Mo^{5+} ions can be highly possible and are expected to participate in the depolymerization of glass network because it creates non-bridging oxygen ions and more bonding defects [26]. The Mo^{5+} ions are essentially coordinated in the studied glasses by five oxygen ligands in a square-pyramidal geometry with a Mo═O double bond. This local vicinity due to the excitation of the Mo^{5+} ions is also confirmed by optical spectra that show two absorption bands situated at about 377 and 714 nm [27].

(v) The addition of MoO_3 up to 30 mol% causes an increase in the intensity of the UV absorption bands situated in the domain between 320 and 450 nm. This noticeable increase can be attributed to the Mo^{3+} and Mo^{6+} ions, in agreement with the EPR and UV–vis spectra. It can be assumed that the molybdenum ions are acting as modifiers in the case of the high MoO_3 content samples and as a consequence, the redox process of the different species of molybdenum ions facilitates a partial transformation of the six-fold coordinate into four-fold coordinate germanium ions followed by formation of GeO_2 and $PbMoO_4$ crystalline phases.

Our results indicate that molybdenum ions occupy different local sites including the presence of Mo^{3+}, Mo^{4+} and Mo^{5+} valence states (where the first one is predominant) depending on the MoO_3 content.

From the observed absorption edges, we have evaluated the optical band gap of these glasses and glass ceramics by drawing the Urbach plot between $h\nu$ and $(\alpha h\nu)^2$. The plots of all these glasses are represented in Fig. 5. Note that a considerable part of each curve was found to be linear. The

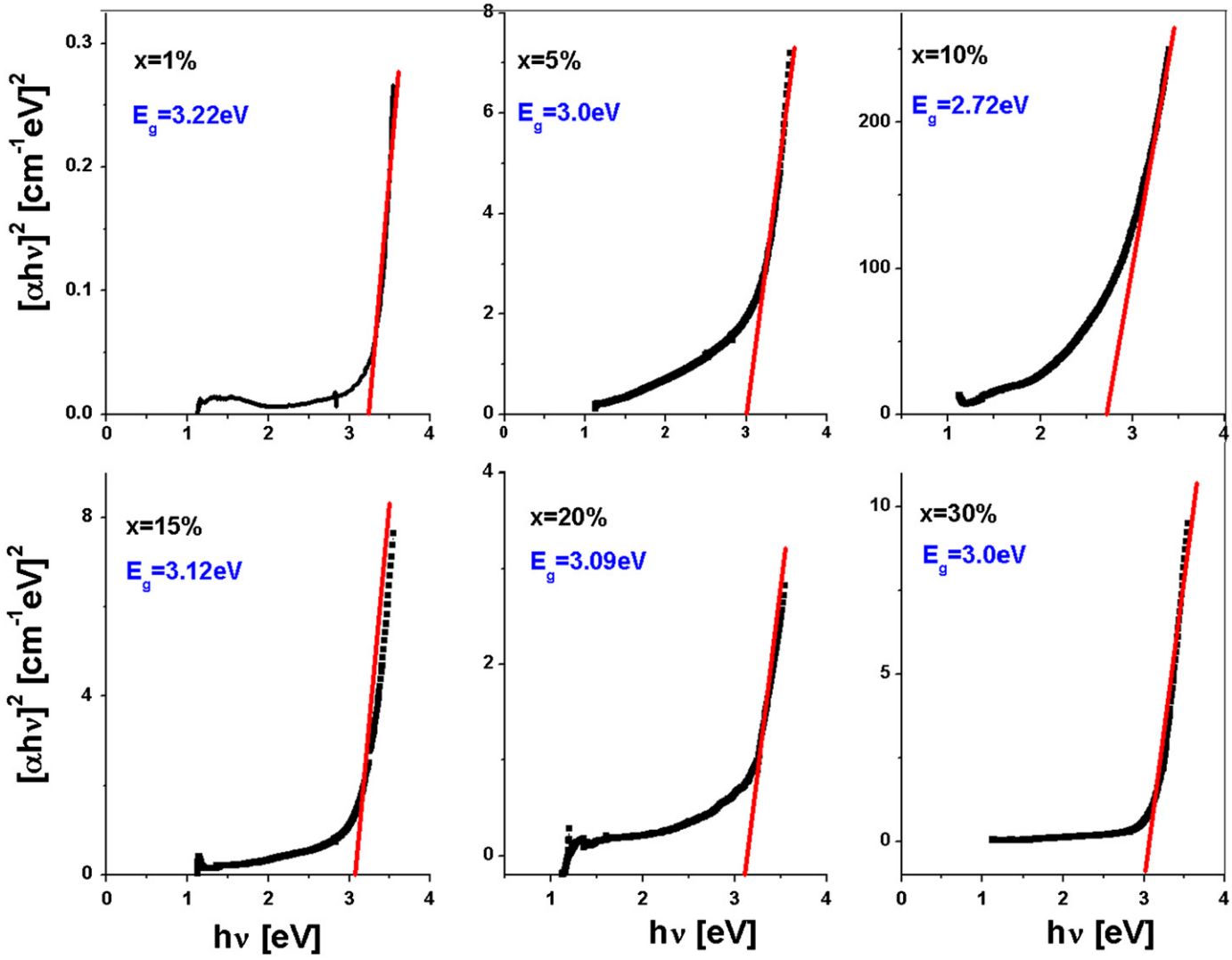

Fig. 5. Plots of $(\alpha h\nu)^2$ versus $h\nu$ for $x MoO_3(100-x)[7TeO_2 \cdot 3PbO]$ glass and glass ceramics samples.

values of optical band gap energy, E_g, were obtained from the extrapolation of linear portions in the plots. The values for the band gap energy decrease gradually from 3.22 to 2.72 eV with the increasing MoO_3 content up to 10 mol%, after that increase (for samples with $10 < x \leq 20$ mol% MoO_3) and finally, decrease again (for sample with $x = 30$ mol% MoO_3).

For the sample with $x = 10$ mol% MoO_3, the lowering of band gap energy suggests that non-bridging oxygen ion concentration increases in the glass network. The non-bridging orbitals have higher energies than the bonding orbitals, contribute to the valence band maximum shifting to higher energies and reduce the band gap. The formation of six-fold coordinate germanium ions reaches a limit, in agreement with density and FTIR data, and the number of non-bridging oxygens begin to increase. The competitive effects of formation of six-fold coordinate germanium ions and non-bridging oxygens lead to the maxima observed.

Independent of the nature of the alkaline ion, the electrical conductivity in the lithium–molybdenum–phosphate glasses was assumed to be due to the electronic hopping from the lower valence state Mo^{5+} ion (donor level) to the higher valence state Mo^{6+} ion (acceptor level) [28]. Further, molybdenum ions are expected to have profound influence on the optical and electrochemical properties of molybdenum–lead-germanate glasses and glass ceramics, in view of the fact that the molybdenum oxide participates in the glass network with different structural units like $[MoO_4]$ tetrahedral structural units, $[MoO_6]$ octahedral units of Mo^{6+} ions and Mo^{5+} ions.

3.4. EPR spectroscopy

The local symmetry and interaction between paramagnetic ions in molybdenum–lead-germanate glasses and glass ceramics can be investigated by EPR spectroscopy. Molybdenum has the electronic configuration [Kr] $4d^5\ 5s^1$. Apparently, Mo^{6+}, Mo^{5+}, Mo^{4+} and Mo^{3+} ions or mixtures of some of them represent the major part of the valence state of molybdenum in glasses. The Mo^{6+} ions with the $4d^\circ$ configuration and the Mo^{4+} ions that posses two 4d electrons gives no EPR spectra. The Mo^{5+} ($4d^1$) and Mo^{3+} ($4d^3$) ions give an EPR signal due to their unpaired electrons.

Fig. 6 illustrates the EPR spectra of some molybdenum–lead-germanate glasses with MoO_3 contents. The shape of the EPR spectra was observed to vary with the increasing MoO_3 content of the samples. For all the studied glasses, the EPR spectra revealed the existence of a signal centered near $g \sim 5.2$. This signal is associated with the presence of Mo^{3+} ions [29,30]. In the case of the studied samples, the EPR spectra show the following important features:

(i) For the samples with $x \leq 10$ mol% MoO_3 the signal located at $g \sim 5.2$ is very intense showing the presence of Mo^{3+} ions.
(ii) By increasing the MoO_3 content of the samples up to $x \geq 15$ mol%, the presence of a small intensity hyperfine structure of the EPR spectra can be observed. This effect is due to the presence of Mo^{5+} ions and not due to paramagnetic impurities [25]. The presence of the hyperfine structure could be an indicative of Mo^{5+}–O–Mo^{6+} bonds disruption in the network.

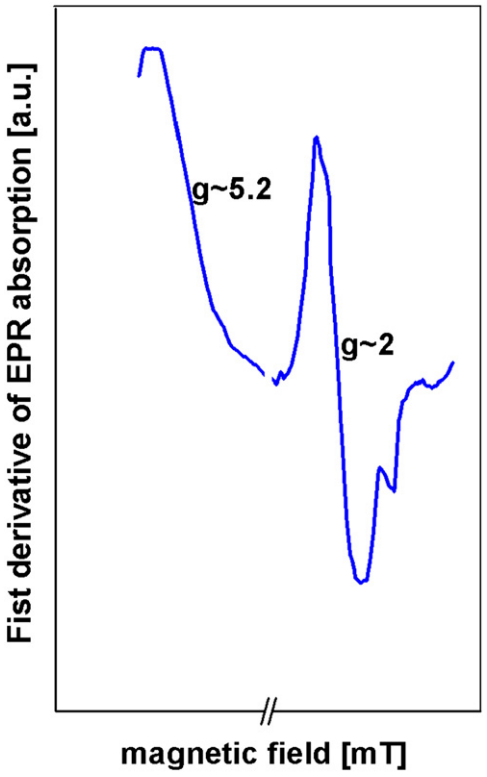

Fig. 6. Optimized structure of the $20MoO_3 \cdot 80[7GeO_2 \cdot 3PbO]$ glasses used to perform the DFT computations.

Some authors show that coordination of Mo^{5+} ions in the glass may be inferred from the symmetry of the EPR spectral line of this ion [31]. If the spectral line is symmetric this corresponds to cubic symmetry around the paramagnetic center. In our case the EPR lines are not highly symmetric showing that the Mo^{5+} ions may be supposed to be in octahedral coordination.

In brief, the microenvironment of molybdenum ions in glasses is expected to have mainly six fold coordination but there is a possibility of reduction of a part of molybdenum ions from the Mo^{6+} to the Mo^{5+} and Mo^{3+} states. These aspects are also correlated with a strong depolymerization of the germanate structure and the formation of GeO_2 and $PbMoO_4$ crystalline phases by increasing the MoO_3 content, in agreement with XRD data.

3.5. DFT studies

The process of doping the host network with molybdenum ions causes changes in the intensity of some FTIR bands but the main characteristic IR features keep their position.

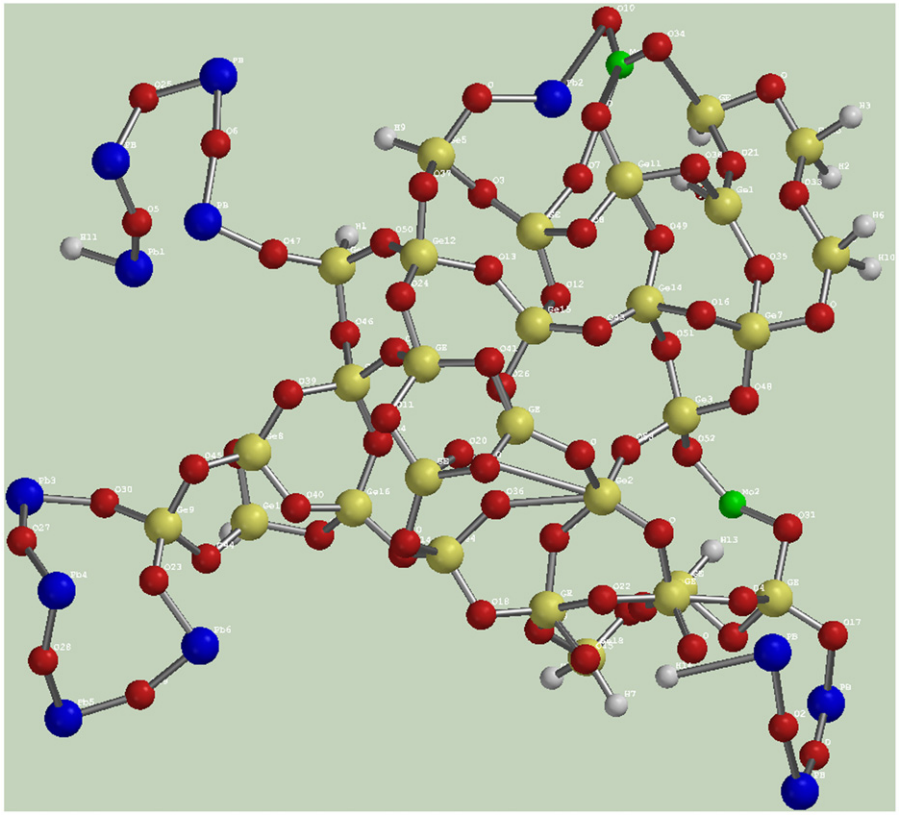

Fig. 7. EPR spectrum for sample with $x=20$ mol% MoO_3.

These changes in the intensities of the IR bands are related to the possible variations in the bond length and bond angles of the vibrating structural units. In this view, quantum chemical calculations will be used in order to understand the local structure of the $20MoO_3 \cdot 80[7GeO_2 \cdot 3PbO]$ glass network. Similar methodology has previously been reported to study other tellurate glasses [32–34].

The structural model obtained for the $20MoO_3 \cdot 80[7GeO_2 \cdot 3PbO]$ glass shown in Fig. 7 gives detailed information concerning the Ge–O, Pb–O framework structure and the environment of molybdenum ions. The model indicates that there is a very small number of $[GeO_6]$ structural units and these have a deformed octahedral geometry. The Ge–O bond length increases its equilibrium value from 1.78–1.81 Å to over 2.61 Å (two Ge–O interatomic distances) equivalent to breaking these bonds. There is instability between the nonequivalent Ge–O bonds in the octahedron and at tridimensional level the tetragonal $[GeO_4]$ structural units becomes favorite.

The Ge–O bonds distances of the square pyramidal $[GeO_5]$ polyhedrons are subdivided into two groups: four bonds have shorter interatomic distances (1.76–1.85 Å) and one has a longer interatomic distance (1.92 Å) than the covalent Ge–O bond length (1.85 Å) but significantly shorter than the sum of the van der Waals radii (3.55 Å).

The Ge–O interatomic distances of the $[GeO_4]$ structural units increase slightly by 0.02–0.07 Å.

By increasing the MoO_3 content up to 20 mol%, we assume that the $[GeO_6]$ structural units do not accommodate with the non-bridging oxygens and also that the $[GeO_5]$ polyhedrons situated in the vicinity of $[GeO_6]$ structural units are highly deformed. In brief, there is a larger displacement of the germanium atom from the center of the square pyramidal and octahedral geometry. Further, at tridimensional level, the observations presented in these mechanisms show that the accommodation of the glass network with the excess of oxygen is possible by formation of GeO_2 crystalline phase with tetragonal $[GeO_4]$ structural units, in agreement with XRD data.

3.6. Electrochemical properties

Electrochemical properties of the molybdenum–lead-germanate glasses and glass ceramics with $x=10$ and 30 mol% MoO_3 were evaluated by the cyclic voltammetry technique. Cyclic voltammograms of the solid-state cells with these glass and glass ceramics after three cycles are shown in Fig. 8. A platinum electrode was used as a counter electrode while the reference was a standard calomel electrode and a glass (or glass ceramics) was used as a working electrode.

For both curves a cathodic current peak was observed. It is situated at about 0.95 V for the sample with $x=10$ mol%MoO_3 and 0.75 V, respectively, for the glass ceramics,

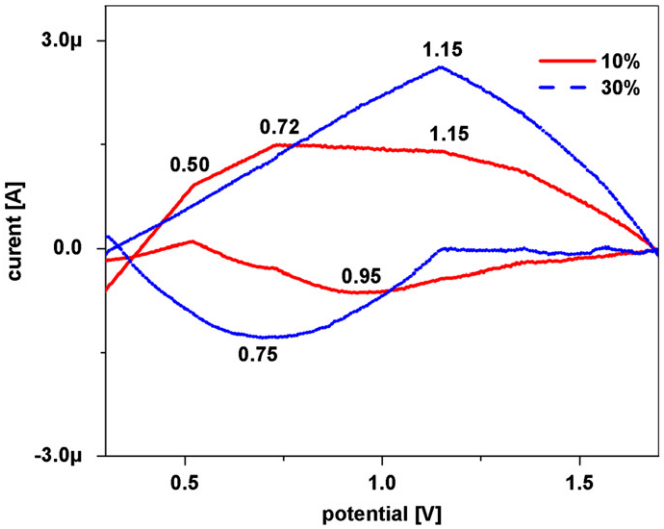

Fig. 8. Cyclic voltammograms of $x\mathrm{MoO_3}\cdot(100-x)\cdot[7\mathrm{GeO_2}\cdot 3\mathrm{PbO}]$ system where $x=10$ and 30 mol% MoO_3 (performed between -2 V and 2 V, for three cycles with a scan rate of 0.1 mV/s in 10^{-5} M $AgNO_3$ aqueous solution).

due to silver deposition. The substitution of 30 mol% MoO_3 in the lead-germanate glass network leads to the decrease of cathodic current in the present study. The difference between these cathodic peaks may be due to the type of electrochemically active species existing in the glass ceramics [35].

Anodic current peaks due to silver dissolution can be observed at about 1.15 V for both samples. The position of the cathodic peak of silver shows more shift with the increasing MoO_3 content up to 30 mol% compared to the anodic peak (the oxidation peak). This indicates that the reduction of the silver occurs more easily than the oxidation process [36]. Some anodic current peaks (situated at about 0.50 and 0.72 V) and a very small cathodic current (situated at about 1.47 V) are observed for sample with $x=10$ mol% MoO_3. In this case, the shape of the peaks was somewhat different from that of glass ceramics.

4. Conclusions

The present work aimed to study the structure and variation of optical band gap, density and molar volume in molybdenum–lead-germanate glass and glass ceramics. The change in density, molar volume and optical band gap was discussed in terms of the structural modifications that take place in the glass matrix with gradual addition of MoO_3.

The spectroscopic studies indicate that with increasing the MoO_3 content, a part of the Mo^{6+} ions are converted into Mo^{3+} and Mo^{5+} ions and this process causes the depolymerization of host glass network. Further, the increase of the MoO_3 content leads to increase of the structural disorder and, accordingly, formation of GeO_2 and $PbMoO_4$ crystalline phases. There are two types of lines in the EPR spectra that correspond to different valences of molybdenum ions in the host network. The concentrations of the paramagnetic centers depend on MoO_3 content and structural properties of the glasses.

Then, we assume that the $[GeO_6]$ structural units do not accommodate with the non-bridging oxygens and that the $[MoO_n]$ polyhedrons are suitable neighbors for the structural units of the lead atoms. For sample $x=20$ mol% MoO_3, the broad absorption bands observed between 370 and 1100 nm in the UV–vis spectrum are attributed to the excitation of Mo^{5+} ions. Probably, due to interchange transition transfer between the Mo^{5+} and Mo^{6+} ions in the glass ceramics network, a smaller resolution of these transitions could be observed by increasing the MoO_3 content up to 30 mol%.

Acknowledgments

The financial support of the Ministry of Education and Research of Romania—National University Research Council (CNCSIS, PN II-IDEI 2012) is gratefully acknowledged by the authors.

References

[1] I. Kashif, Samy A. Rahman, A.G. Mostafa, E.M. Ibrahim, A.M. Sanad, Structural analysis and physical properties of iron–molybdenum–lithium–borate glasses, Journal of Alloys and Compounds 450 (1–2) (2008) 352–358.
[2] L. Bih, L. Abbas, A. Nadiri, H. Khemakhem, B. Elouadi, Investigations of molybdenum redox phenomenon in Li_2O–MoO_3–P_2O_5 phosphate glasses, Journal of Molecular Structure 872 (2008) 1–9.
[3] M.A. Ghauri, S.A. Siddiqi, W.A. Shah, M.G.B. Ashiq, M. Iqbal, Optical properties of zinc molybdenum phosphate glasses, Journal of Non-Crystalline Solids 355 (50–51) (2009) 2466–2471.
[4] L. Abbas, L. Bih, A. Nadiri, Y. El Amraoui, D. Mezzane, B. Elouadi, Properties of mixed Li_2O and Na_2O molybdenum phosphate glasses, Journal of Molecular Structure 876 (1–3) (2008) 194–198.
[5] F.H. ElBatal, A.M. Abdelghany, R.L. Elwan, Structural characterization of gamma irradiated lithium phosphate glasses containing variable amounts of molybdenum, Journal of Molecular Structure 1000 (2011) 103–108.
[6] F.H. ElBatal, Y.M. Hamdy, S.Y. Marzouk, Gamma ray interactions with V_2O_5-doped sodium phosphate glasses, Materials Chemistry and Physics 112 (2008) 991–1000.
[7] A. Ghosh, Temperature-dependent thermoelectric-power of semiconducting bismuth–vanadate glass, Journal of Applied Physics 65 (1989) 227–230.
[8] A. Ghosh, Electrical transport-properties of molybdenum tellurite glassy semiconductors, Philosophical Magazine 61 (1990) 87–96.
[9] S. Mandal, A. Ghosh, Electrical conduction in lead–iron glasses, Journal of Physics: Condensed Matter 8 (1996) 829–836.
[10] M. Sayer, A. Mansingh, Transport properties of semiconducting phosphate glasses, Physical Reviews B 6 (1972) 4629–4643.
[11] C.F. Drake, I.F. Scalan, Bond type, polarisation and electron conduction in some oxide and chalcogenide glasses, Journal of Non-Crystalline Solids 4(C) (1970) 234–247.
[12] Z. Hussain, Optical and electrochromic properties of annealed lithium–molybdenum–bronze thin films, Journal of Electronic Materials 31 (2002) 615–630.

[13] S.M. Abo-Naf, FTIR and UV–vis optical absorption spectra of gamma-irradiated MoO_3-doped lead borate glasses, Journal of Non-Crystalline Solids 358 (2012) 406–413.
[14] S. Hazra, A. Ghosh, Structural properties of unconventional lead cuprate glass, Journal of Materials Research 10 (1995) 2374–2378.
[15] A. Ghosh, Electrical-properties of lead vanadate glasses, Physical Review B 49 (1994) 3131–3135.
[16] M. Scavini, C. Tomasi, A. Speghini, M. Bettinelli, Stable and metastable phases within the GeO_2-rich part of the binary PbO–GeO_2 system, Journal of Materials Synthesis and Processing 9 (2) (2001) 93–102.
[17] Spartan'04, Wavefunction Inc., 18401 Von Karman Avenue, Suite 370 Irvine, CA 92612.
[18] M.J. Frisch, G.W. Trucks, H.B. Schlegel, G.E. Scuseria, M.A. Robb, J.R. Cheeseman, J.A. Montgomery Jr., T. Vreven, K.N. Kudin, J.C. Burant, J.M. Millam, S.S. Iyengar, J. Tomasi, V. Barone, B. Mennucci, M. Cossi, G. Scalmani, N. Rega, G.A. Petersson, H. Nakatsuji, M. Hada, M. Ehara, K. Toyota, R. Fukuda, J. Hasegawa, M. Ishida, T. Nakajima, Y. Honda, O. Kitao, H. Nakai, M. Klene, X. Li, J.E. Knox, H.P. Hratchian, J.B. Cross, C. Adamo, J. Jaramillo, R. Gomperts, R.E. Stratmann, O. Yazyev, A.J. Austin, R. Cammi, C. Pomelli, J.W. Ochterski, P.Y. Ayala, K. Morokuma, G.A. Voth, P. Salvador, J.J. Dannenberg, V.G. Zakrzewski, S. Dapprich, A.D. Daniels, M.C. Strain, O. Farkas, D.K. Malick, A.D. Rabuck, K. Raghavachari, J.B. Foresman, J.V. Ortiz, Q. Cui, A.G. Baboul, S. Clifford, J. Cioslowski, B.B. Stefanov, G. Liu, A. Liashenko, P. Piskorz, I. Komaromi, R.L. Martin, D.J. Fox, T. Keith, M.A. Al-Laham, C.Y. Peng, A. Nanayakkara, M. Challacombe, P.M.W. Gill, B. Johnson, W. Chen, M.W. Wong, C. Gonzalez, J.A. Pople, Gaussian 03, Revision A.1, Gaussian, Inc., Pittsburgh, PA, 2003.
[19] S. Rada, M. Rada, E. Culea, Structural and optical properties of the gadolinium–lead–germanate glasses, Journal of Non-Crystalline Solids 357 (1) (2011) 62–66.
[20] S. Rada, E. Culea, Structural and optical properties in gadolinium–aluminum–lead–germanate quaternary glasses, Journal of Non-Crystalline Solids 357 (7) (2011) 1724–1728.
[21] S. Rada, R. Chelcea, E. Culea, Experimental and theoretical investigations on the structure–properties interrelationship of the gadolinium–vanadate–germanate glasses, Journal of Molecular Modeling 17 (2011) 165–171.
[22] S. Rada, E. Culea, Novel photosensitive properties of gadolinium–lead germanate glasses, Molecular Physics 108 (14) (2010) 1877–1886.
[23] M. Rada, V. Maties, M. Culea, S. Rada, E. Culea, Dual role of the six-coordinated molybdenum and lead ions in novel of photochromic properties of the molybdenum–lead–borate glasses, Spectrochimica Acta Part A 75 (2010) 507–510.
[24] M. Rada, S. Rada, P. Pascuta, E. Culea, Structural properties of molybdenum–lead–borate glasses, Spectrochimica Acta Part A 77 (4) (2010) 832–837.
[25] R. Ciceo Lucacel, A.O. Hulpus, V. Simon, Structural characterization of phosphate glasses doped with silver, Journal of Non-Crystalline Solids 355 (2009) 425–429.
[26] S.B.M. Krishna, A.R. Babu, R.Ch. Sree, D.K. Rao, Influence of molybdenum ions on the structure of ZnO–As_2O_3–Sb_2O_3 glass system by means of spectroscopic and dielectric studies, Journal of Non-Crystalline Solids 356 (2010) 1754–1761.
[27] O. Cozar, I. Ardelean, S. Simon, L. David, ESR studies of Mo^{5+} ions in potassium-borate and soda-phosphate glasses, Solid State Communications 85 (5) (1993) 461–465.
[28] O. Cozar, D.A. Magdas, I. Ardelean, EPR study of molybdenum–lead–phosphate glasses, Journal of Non-Crystalline Solids 354 (2008) 1032–1035.
[29] F. Farges, R. Siewert, G.E. Brown, A. Guesdon, Structural environments around molybdenum in silicate glasses and melts I. Influence of composition and oxygen fugacity on the local structure of molybdenum, Canadian Mineralogist 44 (2006) 731–753.
[30] R.J. Landry, ESR and optical absorption study of Mo^{3+} in a phosphate glass, Journal of Chemical Physics 48 (1968) 1422–1423.
[31] S. Simon, Al. Nicula, Magnetic resonance of the B_2O_3–Na_2O–MoO_3 vitreous system, Journal of Non-Crystalline Solids 57 (1983) 23–29.
[32] S. Rada, M. Culea, M. Neumann, E. Culea, Structural role of europium ions in lead-borate glasses inferred from spectroscopic and DFT studies, Chemical Physics Letters 460 (2008) 196–199.
[33] S. Rada, M. Culea, E. Culea, Toward modeling phosphate tellurate glasses: the devitrification and addition of gadolinium ions behavior, Journal of Physical Chemistry A 112 (44) (2008) 11251–11255.
[34] S. Rada, E. Culea, FTIR spectroscopic and DFT theoretical study on structure of europium–phosphate–tellurate glasses and glass ceramics, Journal of Molecular Structure 929 (2009) 141–148.
[35] K. Minami, A. Hayashi, S. Ujiie, M. Tatsumisago, Electrical and electrochemical properties of glass-ceramic electrolytes in the systems Li_2S–P_2S_5–P_2S_3 and Li_2S–P_2S_5–P_2O_5, Solid State Ionics 192 (2011) 122–125.
[36] K.S. Kim, S.J. Park, Influence of silver-decorated multi-walled carbon nanotubes on electrochemical performance of polyaniline-based electrodes, Journal of Solid State Chemistry 184 (2011) 2724–2730.